

See discussions, stats, and author profiles for this publication at: <https://www.researchgate.net/publication/230614460>

# Transient Fibril Structures Facilitating Nonenzymatic Self-Replication

ARTICLE *in* ACS NANO · AUGUST 2012

Impact Factor: 12.88 · DOI: 10.1021/nn302223v · Source: PubMed

---

CITATIONS

19

READS

62

## 6 AUTHORS, INCLUDING:



Boris Rubinov

ADAMA Agricultural Solutions Ltd

15 PUBLICATIONS 121 CITATIONS

[SEE PROFILE](#)



Nathaniel Wagner

Ben-Gurion University of the Negev

29 PUBLICATIONS 328 CITATIONS

[SEE PROFILE](#)



Maayan Matmor

Ben-Gurion University of the Negev

10 PUBLICATIONS 75 CITATIONS

[SEE PROFILE](#)



Nurit Ashkenasy

Ben-Gurion University of the Negev

45 PUBLICATIONS 824 CITATIONS

[SEE PROFILE](#)

# Transient Fibril Structures Facilitating Nonenzymatic Self-Replication

Boris Rubinov,<sup>†</sup> Nathaniel Wagner,<sup>†,II</sup> Maayan Matmor,<sup>‡</sup> Oren Regev,<sup>§,⊥</sup> Nurit Ashkenasy,<sup>‡,⊥</sup> and Gonen Ashkenasy<sup>†,\*</sup>

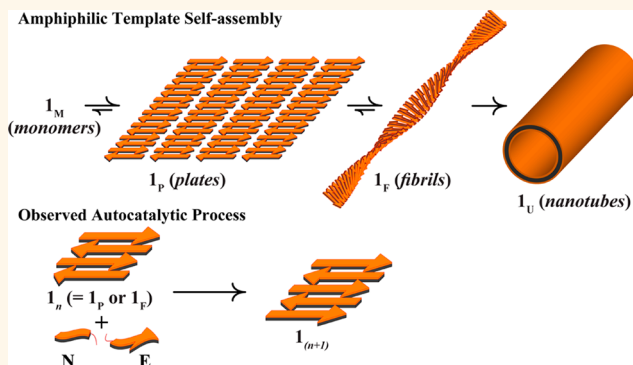
<sup>†</sup>Department of Chemistry, <sup>‡</sup>Department of Materials Engineering, <sup>§</sup>Department of Chemical Engineering, and <sup>⊥</sup>Ilse Katz Institute for Nanoscale Science and Technology, Ben Gurion University of the Negev, Beer Sheva, Israel and <sup>II</sup>IYAR, Israel Institute for Advanced Research, Rehovot, Israel

Self-assembly of amphiphilic biomolecules, such as fatty acids, peptides, and proteins, has been the subject of intense research, with implications for supramolecular chemistry, cell biology, and nanotechnology. It has been shown that these molecules can form different structures in water, including elongated fibril-type or nanotube structures, and that the functions of these structures depend closely on different parameters such as the aggregates' size, their architecture at the nanoscale, the interface with the surroundings, and interactions with other molecules in the mixtures.<sup>1–12</sup> An interesting new direction of research that may benefit from the ability to control the assembly of amphiphilic molecules into large structures focuses on developing “self-synthesizing materials”,<sup>13–15</sup> molecular assemblies that upon request can promote their own formation by accelerating the synthesis of their building blocks and/or the assembly of their superstructures. We describe here the self-assembly of short amphiphilic peptides into various forms of soluble  $\beta$ -sheet nanostructures and the consequent activity of the latter as autocatalysts for synthesis of monomeric peptides from simpler building blocks.

Nonenzymatic molecular replication was first introduced in the mid-1980s using synthetic DNA molecules<sup>16</sup> and, since then, has also been demonstrated with RNA, peptides, and small organic molecules.<sup>17–20</sup>

The studies of such molecules were conducted originally to shine light on the basic principles of catalysis and to probe scenarios relevant to the origin of life<sup>17,20</sup> and have been recently expanded for finding new tools to control complex reaction networks<sup>18,21,22</sup> and to synthesize structures that might be useful for nanotechnology.<sup>13,23,24</sup> In most of the studied replication systems, a single molecule or small dimeric complexes have served as the catalytic species, i.e.,

## ABSTRACT



An emerging new direction of research focuses on developing “self-synthesizing materials”, those supramolecular structures that can promote their own formation by accelerating the synthesis of building blocks and/or an entire assembly. It was postulated recently that practical design of such systems can benefit from the ability to control the assembly of amphiphilic molecules into nanostructures. We describe here the self-assembly pathway of short amphiphilic peptides into various forms of soluble  $\beta$ -sheet structures— $\beta$ -plates, fibrils, and hollow nanotubes—and their consequent activity as autocatalysts for the synthesis of monomeric peptides from simpler building blocks. A detailed kinetic analysis of both the self-assembly and self-replication processes allows us to suggest a full model and simulate the replication process, revealing that only specific structures, primarily fibrils that are stable within the solution for a time shorter than a few hours, can be active as catalysts. Interestingly, we have found that such a process also induces fibril reproduction, in a mechanism very similar to the propagation of prion proteins by transmission of misfolded states.

**KEYWORDS:** systems chemistry · self-replication ·  $\beta$ -sheet · fibrils · prion proteins

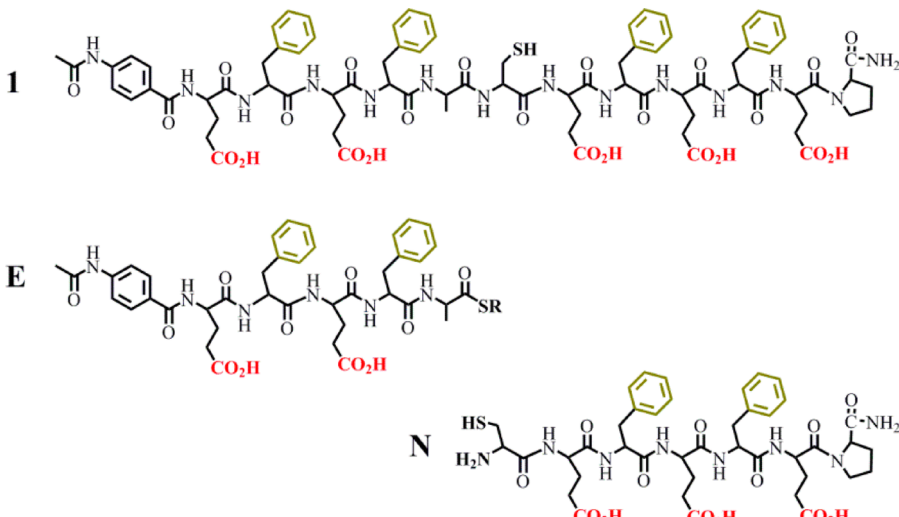
templates for noncovalent binding of substrate molecules accelerating their attachment via a ligation reaction. In particular, peptide self-replication has been described by several groups, including the authors, using monomeric or dimeric  $\alpha$ -helix peptides as the templates.<sup>25–27</sup> These  $\alpha$ -helix peptides consisted of relatively long sequences (>30 amino acids) and defined

\* Address correspondence to gonenash@bgu.ac.il.

Received for review May 20, 2012 and accepted August 2, 2012.

Published online August 02, 2012  
10.1021/nn302223v

© 2012 American Chemical Society



**Scheme 1.** Chemical structures of the self-replicating peptide **1** and its electrophilic (**E**) and nucleophilic (**N**) fragment precursors readily activated for native chemical ligation. Peptides consist of the native L-type  $\alpha$ -amino acids.

three-dimensional structures. We study here the replication of a much simpler amphiphilic peptide (**1**; see sequence in Scheme 1) that can accelerate its own formation from a solution containing electrophilic and nucleophilic precursors (**E** and **N**, respectively; Scheme 1).<sup>28</sup> It is made of 13 amino acids, alternating Glu and Phe residues, an Ala-Cys ligation site in the middle, and “capping” proline groups at both ends that can promote 1D aggregation.<sup>29</sup> Since the monomeric form of **1** cannot adopt a defined three-dimensional structure in water, we have postulated that 1D  $\beta$ -sheet nanostructures formed in the solution serve as supramolecular templates for the reaction. In particular, we are suggesting that fibrillar structures can facilitate the association of the precursors **E** and **N** by binding them temporarily at the many edges of the growing structures, as illustrated, for example, by a cryogenic transmission electron microscopy (cryo-TEM) micrograph recorded during the self-assembly of **1** (Figure S1a, Supporting Information). The paper describes a detailed study directed at elucidating the kinetics of formation of soluble  $\beta$ -sheet structures of **1**, including  $\beta$ -plates, fibrils, and hollow nanotubes. Using a battery of analytical tools we analyze transitions between these different supramolecular structures, and by correlating these with new kinetic experiments we find that the fibrillar structures are the most accessible templates in the time window relevant to the replication reaction. With this information, we are able to suggest a full kinetic model and simulate the replication process, when taking into consideration fibril growth, fibril dissociation, and transition into the inactive tubular phase, synchronized with the ligation processes aided by the fibrils. Interestingly, we have found from this modeling that the process induces fibril reproduction in a mechanism very similar to the information transfer mechanism observed for prion

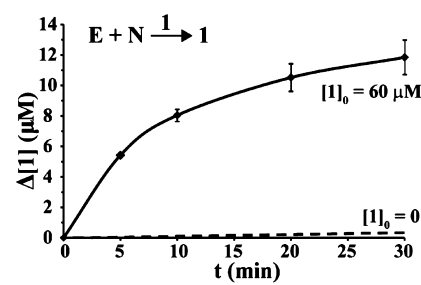


**Figure 1.** Kinetic profile observed for production of **1** over time in reactions between equimolar amounts of **E** and **N** (250  $\mu$ M each). The template-seeded ( $[1] = 60 \mu$ M) and template-free (dashed black line; interpolation of data collected at longer times) reactions were performed in buffer at pH 7 with tris(2-carboxyethyl)phosphine hydrochloride (TCEP) as reducing agent and a foreign peptide labeled with 4-acetamido benzoate (ABA) as a standard. Product concentrations were derived from RP-HPLC chromatograms of aliquots collected along the reaction.

proteins. It is noticeable that this study provides a unique example of the crucial role of the reactivity of transient nanostructures formed by self-assembly processes through weak bonds and shows that careful synchronization between the kinetics of the self-assembly process and the desired activity (template-assisted ligation in our case) can improve the function significantly.

## RESULTS AND DISCUSSION

The results shown in Figure 1 are given as an example of the rate enhancement observed when the ligation of **E** and **N** is initiated in the presence of **1** (~25 mol %) as a template, relative to the template-free reaction rate. The following experiments and then the theoretical analysis were conducted in order to probe the dependence of the replication reaction on self-assembly of template **1** and the catalytic ability of the nanostructure that are formed *in situ*.

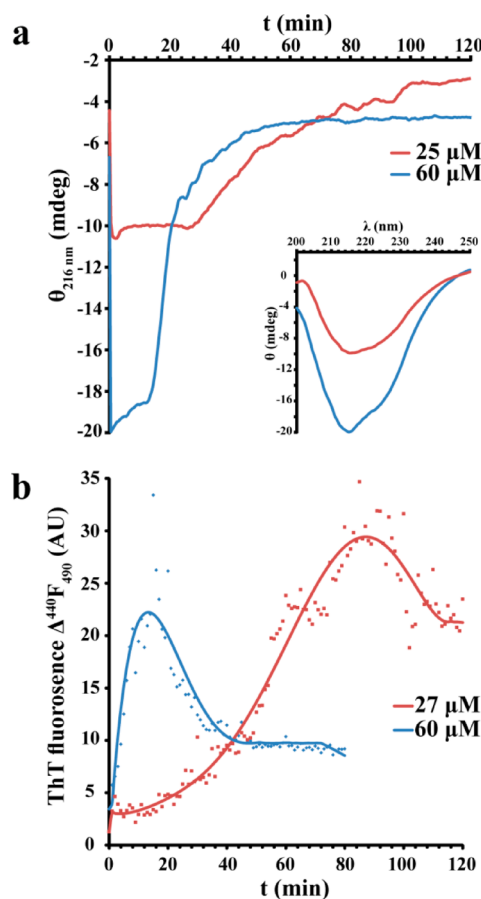


**Figure 2.** Kinetic analysis of the self-assembly process of peptide 1. (a) CD ellipticity at 216 nm as a function of time for 25 and 60  $\mu\text{M}$  solutions of 1. Inset: CD spectra of 1 obtained 1 min after sonication. (b) ThT fluorescence over time for 27 and 60  $\mu\text{M}$  solutions of 1. Experiments performed after vigorous sonication of solutions of 1 in the indicated concentration in 20 mM 3-(*N*-morpholino)-propanesulfonic acid (MOPS) buffer at pH 7 and with TCEP as a reducing agent.

**Analyzing the Self-Assembly Pathway of Template 1.** The self-assembly of 1 in neutral aqueous solutions was analyzed over time using a battery of analytical techniques. It has been shown previously that amphiphilic peptide sequences can form monolayer assemblies at the air–water interface,<sup>30</sup> and we have thus further analyzed here the formation of soluble structures. Solutions of 1 (10–100  $\mu\text{M}$ ) in buffer at pH 7 were first equilibrated after their vigorous sonication (at 40 kHz for  $\geq 10$  min). At various time points aliquots were centrifuged and the supernatant was injected into the HPLC. Very small changes in peptide concentrations were observed over the course of 3 h (Figure S2), confirming the existence of perfectly soluble structures under the studied conditions. Circular dichroism (CD) measurements of low (25  $\mu\text{M}$ ) and higher (60  $\mu\text{M}$ ) concentrations of 1 after short equilibration time (1 min) showed the typical spectra of  $\beta$ -sheet structures, with the indicative minima at 216 nm (Figure 2a, inset). Following the changes in ellipticity at 216 nm

minima during the course of 2 h (Figure 2a) revealed an increase in signal, corresponding to phase transitions between different  $\beta$ -sheet-containing structures.<sup>31,32</sup> As expected, the transition had occurred earlier for the more concentrated solution,  $\sim 15$  and 30 min for 60 and 25  $\mu\text{M}$  solutions, respectively. In addition, we observed a sharper increase in signal for the 60  $\mu\text{M}$  solution due to the faster transition that had taken place. CD spectra of both solutions after 2 h showed low ellipticity at 216 nm and formation of new minima at 230 nm, which can be attributed to helical superstructures (Figure S3).<sup>32</sup> A similar behavior, namely, fast assembly and earlier phase transitions for the more concentrated solution (60  $\mu\text{M}$ ), relative to the less-concentrated one (27  $\mu\text{M}$ ), was observed when we characterized the self-assembly of 1 using the fluorescence-based thioflavin T (ThT) assay (Figure 2b), which reports on formation of amyloid-like structures for molecules that self-assemble into fibers. The (490 nm) fluorescence increases at early stages and then starts to decrease, after 20 and 90 min, for the 60 and 27  $\mu\text{M}$  solutions, respectively. This observation can be attributed to formation of a new phase (nanotubes; *vide infra*) or alternatively to self-quenching between closely positioned ThT molecules bound to the fibrils. The difference in transition times observed for the CD and ThT measurements is attributed to the inherent differences between the two assays, and in particular to the fact that in the latter experiment the ThT molecules should first be associated with the fibrils, in a diffusion-limited process, before signal is observed.

We have further characterized the time-dependent formation of supramolecular structures of 1 over the course of several hours by taking electron microscopy images of vitrified samples (by Cryo-TEM) at various time points after vigorous sonication of 60  $\mu\text{M}$  solutions in buffer at pH 7 (Figure 3). The measurements right after the sonication (Figure 3a) showed no particular structures, but rather “islands” of amorphous powder. After a short time of equilibration ( $\sim 15$  min), large  $\beta$ -plate assemblies, made of elongated structures with measured interstrand distances of  $\sim 5.5$  nm, which correspond well with the measured molecular length of 1, were observed (Figure 3b). After longer times of equilibration (30–60 min after sonication), we observed predominantly fibril structures (Figures S1a, 3c, and 4a) made of monofibrils and/or wider fibril bundles. When the system allowed equilibrating for considerably longer times (2 h to overnight), we mainly observed the formation of wider hollow tubular assemblies (Figure 3d).

Since the formation of fibril structures is dominant in the time window relevant to the kinetic experiments, usually done over 1–3 h, we have decided to analyze these species in more detail (Figure 4). As evident from the example shown in Figure 4a, at 60 min after sonication the system consisted of fibrils with different

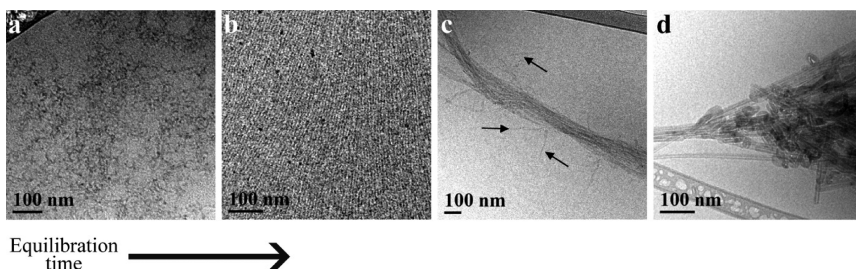


**Figure 3.** Cryo-TEM micrographs of vitrified structures formed in  $60\ \mu\text{M}$  solutions of **1** in MOPS buffer at pH 7, obtained immediately (a) or 15 min (b), 60 min (c), and 120 min (d) after sonication. Arrows in panel (c) are pointing to narrow monofibrils. Additional images showing fibrils and nanotubes are given in the Supporting Information (Figure S1).

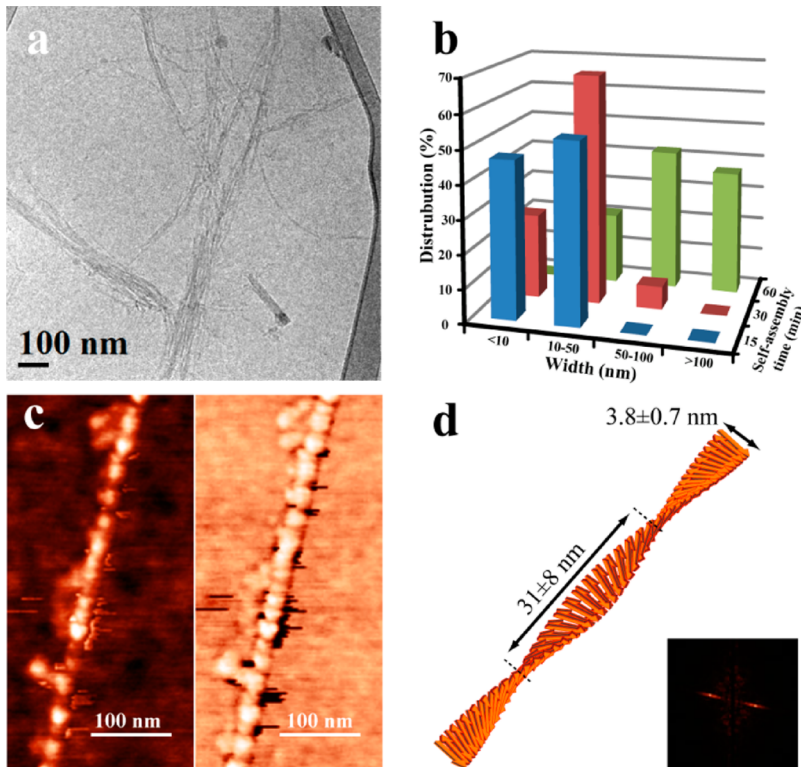


**Figure 4.** Detailed characterization of the fibril structures formed by peptide **1**. (a) Sample cryo-TEM image showing fibrilar structures of different sizes found 60 min after sonication. (b) Statistical analysis of fibrilar structure widths in cryo-TEM micrographs as a function of equilibration time. (c) AFM image, topography (left) and phase (right), of a monofibril formed in a  $60\ \mu\text{M}$  solution of **1** in buffer at pH 7. (d) Analysis of fiber dimensions as obtained from statistics on a large number of AFM measurements. Inset: Fourier transformed diffraction pattern evidencing the repetitive helical features in the fibrillar structure.

morphologies, isolated fibrils with a width of  $\sim 5\ \text{nm}$  and bundled fibrils of different widths up to more than  $100\ \text{nm}$ . A reasonable assumption for the self-assembly pathway would be that monofibrils are first formed and then aligned side-by-side to coil around each other, forming wider bundles.<sup>33,34</sup> Indeed, when statistical analysis of multiple samples, each containing several fibrils, was done to follow the process of fibril widening over time (Figure 4b), we observed that while only narrow fibrils were formed at short times after sonication, at 2 h after sonication, or more, only wide fibers existed. Noticeably, the wide fibers were found to be even thicker than the nanotubes formed at these later stages, with width almost twice as large as the

nanotube diameter, a fact that was described before as driven *via* packing of the less ordered fibrils to form the nanotubes.<sup>34</sup> To further analyze the fibril structure, we have characterized monofibrils formed in  $60\ \mu\text{M}$  solutions in higher height resolution using atomic force microscopy (AFM; Figure 4c) and were able to reconfirm that the width of the monofibril correlates well with that of the length of the monomer and the diameter obtained by our cryo-TEM measurements (Figure 3c). Interestingly, we were also able to extract the dimensions of the pitch ( $31\ \text{nm}$ ) obtained for the coiling of the elongated monofibril structure.

**Correlating Template Self-Assembly with the Replication Kinetics.** We have already established that the rate of

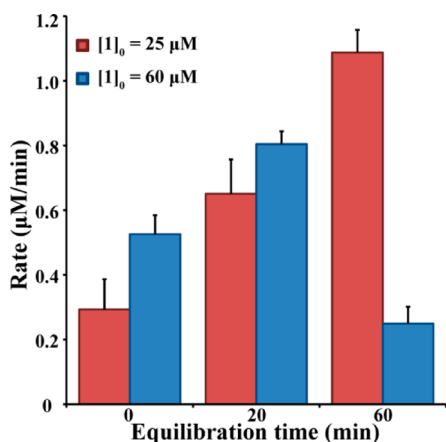


**Figure 5.** Rate of formation of **1** in template-seeded reactions as a function of equilibration self-assembly time. Reactions were performed with 250  $\mu\text{M}$  precursors (**E** and **N**) at room temperature in MOPS buffer at pH 7 and with TCEP as a reducing agent. The experiments were initiated at different time points after sonication (immediately, 20 and 60 min). The amounts of formed product were determined by RP-HPLC (see example in Figure S5), using a foreign ABA-labeled peptide as a standard.

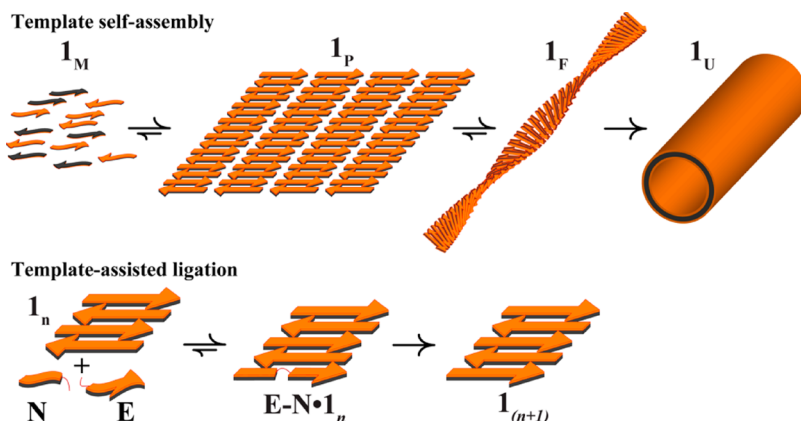
ligation of **E** and **N** to form a new copy of **1** is enhanced when the reaction is initiated in the presence of **1** itself, reflecting an efficient autocatalytic process. The reaction order with respect to starting materials was found here to be 1, as calculated from the kinetic experiment with various concentrations of **E** (Figure S4a). Furthermore, the autocatalysis is specific in that mutants of peptide **1** that cannot form  $\beta$ -sheets do not replicate.<sup>28</sup> In order to obtain a better understanding of the replication mechanism, using the above disclosed data on the template self-assembly, we looked to analyze which one (or more) of the available  $\beta$ -sheet phases possesses better autocatalytic properties. To that end, we ran replication experiments in which we followed the reaction between **E** and **N** (250  $\mu\text{M}$  each) several times with two different concentrations of **1** as a template and by initiating the reaction at different times after vigorous sonication of the solution (Figure 5). The observed initial rates revealed that extending the equilibration time up to 60 min, for reactions seeded with 25  $\mu\text{M}$  of **1**, increased the rate of the reaction. Furthermore, analyzing multiple runs with different concentrations of seeded template, using the common logarithmic treatment (Figure S4b and c, Supporting Information),<sup>35</sup> showed that template equilibration for 20 min increases the replication reaction order to  $p = 1.2$ , relative to reactions for which the template was seeded immediately after its sonication ( $p = 0.9$ ). The rate of reactions seeded with 60  $\mu\text{M}$  **1** increased when seeded after 20 min of equilibration, relative to reactions with no equilibration. Then, longer equilibration times (60 min) resulted in a decrease in the rate, due probably to transition of the template into a noncatalytically active phase containing the nanotubes.

Taken together, the self-assembly and replication kinetic data allowed us to conclude that molecule **1** can serve as an active template for a certain amount of time after its solubility, when certain species, predominately  $\beta$ -plates and fibrils, exist in the mixture. Scheme 2 thus describes the two-level mechanism suggested to reflect the template polymerization, in which catalytic species of **1** are formed during self-assembly (top) and serve as templates and catalysts for ligation of the precursors to form new copies of **1** (bottom). This description allows us to suggest a kinetic model that can be used to describe the observed progress of the reaction.

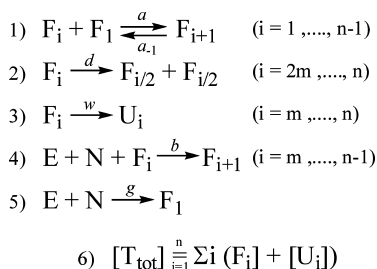
#### Modeling the Simultaneous Self-Assembly and Replication Reactions.

Scheme 3 presents the kinetic model we have used to describe the processes shown in Scheme 2, simplified in that only one type of transient species, the fibril **F**, is considered as a catalyst for the replication. The first three reactions, eqs 1 to 3, refer to the self-assembly of the peptides into fibril and nanotube structures, and the two other reactions, eqs 4 and 5, account for the peptide self-replication. The growth of a fibrillar structure is given in eq 1, describing the reversible association of  $F_i$ , a fibril of length  $i$ , together with a monomeric peptide  $F_1$ , into  $F_{i+1}$ , a fibril of length  $i+1$ . Equation 2 describes the dissociation of a relatively long fibril  $F_i$  into two shorter fibrils  $F_{i/2}$ , and eq 3 describes the irreversible transformation of a fibril  $F_i$  into a corresponding nanotube  $U_i$ . The replication process is then described as a ligation reaction of **E** and **N** aided by a fibril template  $F_i$  (eq 4), accompanied by a slow background template-free ligation (eq 5). According to our analysis using the simulation (below), this is the minimal mechanism required to describe the overall self-assembly-driven replication of peptide **1**. Note that only fibrils with minimal “seeds” of length  $m$  are considered as species of relatively long half-lives, capable of acting as templates or capable of transforming into nanotubes (eqs 3 and 4). Likewise, only longer fibrils ( $i \geq 2m$ ) are considered to be capable of (symmetric) dissociation (eq 2). Interestingly we found that the fibril decomposition step (eq 2) is necessary in order to summarize the transitions among the various forms of catalytic templates in Scheme 2, namely, **1<sub>P</sub>** and **1<sub>F</sub>** of various sizes.

On the basis of the kinetic model in Scheme 3, we ran a simulation in Matlab in the following manner. First, the system is seeded only with monomeric strands ( $F_1$ ), and only the self-assembly reactions (eqs 1–3) are implemented, allowing the system to form the different aggregates. Then, at a preset time of template equilibration, the fragments **E** and **N** are seeded, and all reactions (eqs 1–5) are implemented in parallel. At every time step, after the initial template equilibration time, the various concentrations are computed. The total concentration of template ( $[T_{\text{tot}}]$ ) is the sum over all strands of the fibrils  $F_i$  and the nanotubes



**Scheme 2.** Schematic representation of the two processes that take place in parallel during replication. (Top) Dynamic self-assembly of monomers ( $1_M$ ) to anti-parallel  $\beta$ -pleated sheets ( $1_P$ ), fibers ( $1_F$ ), and finally nanotubes ( $1_U$ ). (Bottom) Autocatalytic reaction in which the  $\beta$ -sheet structure (generally depicted as  $1_n$ ) serves as a template for registered association of  $E$  and  $N$ , which then react to form a new copy of  $1$  and the larger aggregate ( $1_{n+1}$ ), available to serve again as a template



**Scheme 3.** Kinetic model used to describe the replication process shown in Scheme 2.

$U_i$  (eq 6). The system was simulated many times using experimentally relevant initial concentrations of  $E$  and  $N$  (250  $\mu\text{M}$  each) and  $F$  (0–100  $\mu\text{M}$ ) and reasonable values for  $m$  and  $n$  (10 and 100, respectively) and for the rate constants  $a$ ,  $a_{-1}$ ,  $d$ ,  $w$ ,  $b$ , and  $g$ .<sup>36</sup> Representative results displaying the progress of the reactions for using such parameters are shown in Figure 6. Figure 6a displays the growth of the total template concentration as a function of time for two initial monomer fibril concentrations  $F_1$ , 15 and 60  $\mu\text{M}$ , after being allowed to equilibrate for a selected time ( $t = 250$  s). The general profile of product formation and the relative rate enhancement for the two concentrations fit well with the observed experimental patterns. Figure 6b shows a snapshot of the product concentrations at a specific time ( $t = 400$  s) for these two initial concentrations of  $F_1$ , with each showing three separate values for different template equilibrium times. As expected, the higher initial concentration of  $F_1$  yields higher product formation. Similarly, higher values for the template equilibrium time generally yield higher concentrations, since the longer times allow further aggregation into the catalytically active templates. An exception, however, is seen for  $F_1 = 60 \mu\text{M}$  after a long equilibration time of 2500 s. In this case, the longer aggregation time allowed significant formation of the catalytically inactive nanotubes, yielding a lower concentration than the corresponding case after a template equilibration

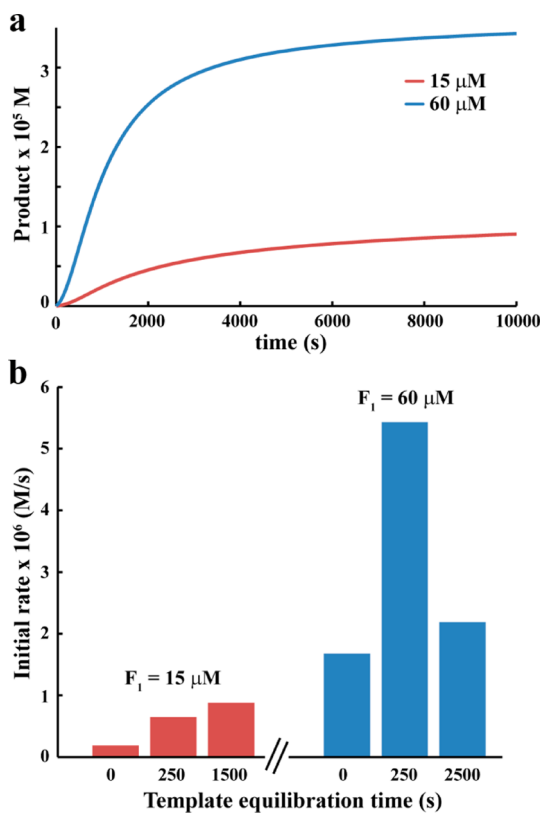


**Figure 6.** Simulation results based on the mechanism shown in Scheme 3, using experimental initial concentration values for  $E$ ,  $N$  (250  $\mu\text{M}$  each) and  $F$ ;  $m$  and  $n$  values of 10 and 100, respectively; and rate constants  $a$ ,  $a_{-1}$ ,  $d$ ,  $w$ ,  $b$ , and  $g$  of  $10^4$ ,  $10^{-2}$ ,  $10^{-2}$ ,  $10^{-2}$ ,  $10^6$ , and  $10^{-3}$ , respectively. (a) Product concentration as a function of time for two initially seeded concentrations of fibril  $F_1$ , 15 and 60  $\mu\text{M}$ , in reactions started after a template equilibrium time of 250 s. Product concentrations were calculated by subtracting  $F_1$  initial concentration from  $[T_{\text{tot}}]$ , the sum over all fibrils  $F_i$  and nanotubes  $U_i$  concentrations, calculated for each time point according to eq 6 in Scheme 3. (b) Snapshot of the concentrations at time  $t = 400$  s (given as the initial rate) for the two initial concentrations of  $F_1$  as a function of template equilibration times.

time of 250 s. This, too, is consistent with the above-described experimental results. We note that our

model can also be useful to track length distribution among the fibril species. This structural characterization may also be achievable by further analyzing the electron microscopy data and is suggested for future research.

Recent works have suggested a mechanistic explanation for how prion proteins propagate in diseases that affect the structure of the brain or other neural tissues, by transmitting a misfolded protein state.<sup>37–39</sup> These mechanisms illustrate the pathological cascade that leads from the properly soluble protein to the accumulation of its insoluble aggregates composed of fibrillar structures. Our mechanism for template polymerization of simple amphiphilic peptides shows a similarity to that of the prions. Both systems undergo conversion of soluble proteins into monomeric units with high tendency to form  $\beta$ -sheet assemblies, which in turn act as nuclei for the self-replication steps. Some differences between the two mechanisms can also be pointed out. The major difference is that the prions form new copies in equilibrium, governed by partially unfolded proteins,<sup>40</sup> while the synthesis of peptide **1** in our model is nonreversible, due to the formation of a covalent amide bond. Additionally, while in prions the reaction decay is a result of the dilution of catalytically active aggregates into soluble proteins, the decay in catalysis in our system is due to the conversion of the

aggregates into other supramolecular structures, i.e., nanotubes.

## SUMMARY AND CONCLUSIONS

We have described in this paper the self-assembly-driven template polymerization and replication of simple amphiphilic peptides. It is clear from the molecular structure of peptide **1**, and well-supported by our results, that the monomeric form cannot serve as a template for the ligation of **E** and **N**, and thus the assembly into  $\beta$ -sheet nanostructures is crucial for its function. Several recent essays have discussed the potential roles of  $\beta$ -sheets made of simple peptides in prebiotic environments, highlighting mainly their effective protection against decomposition or racemization of polyribonucleotides and polypeptides and their catalytic activity.<sup>41,42</sup> Other groups have shown that  $\beta$ -sheet templates can affect enzyme-assisted amino acid polymerization<sup>43</sup> and replication of cyclic peptide structures.<sup>44</sup> Additionally, chiral amplification via peptide polymerization was observed and associated with the formation of racemic (parallel or antiparallel)  $\beta$ -sheets from isotactic strands.<sup>45</sup> Our study adds valuable information to this line of research, by highlighting that the observed function may, and sometimes should, be associated with short-lived  $\beta$ -sheet superstructures.

## EXPERIMENTAL SECTION

**Synthesis and Sample Preparation.** Peptides **1** and **N** were synthesized on solid phase using Rink-Amide resin with Fmoc-based chemistry. Peptide **E** was synthesized on MBHA resin functionalized with Boc-Ala-S(CH<sub>2</sub>)<sub>2</sub>CO<sub>2</sub>H by using Boc-based chemistry. All peptides were purified by preparative RP-HPLC, with a step gradient of solvents A (0.1 M NH<sub>4</sub>HCO<sub>3</sub> in water; pH = 8) and B (acetonitrile). The identity and purity of the peptides were then analyzed by analytical HPLC, MALDI-TOF MS, and LCMS.

Stock solutions of about 1 mM peptide **1**, used for all structural characterizations (CD, AFM, cryo-TEM, and ThT assays), were prepared by weighing lyophilized peptides into Eppendorf tubes, dissolution in Millipore water/ACN (50/50%), and then sonication (at 40 kHz) for 10 min. Then, the peptide was diluted again in MOPS buffer at pH = 7 to the desired concentration. The exact final concentration of each peptide solution was determined from its UV absorbance at 270 nm, based on the extinction coefficient of ABA. The diluted solution was further sonicated for 10 min in order to achieve full disassembly of peptide **1** aggregates to monomers. The structural characterizations and self-assembly-dependent replication experiments were initiated at different times after the sonication.

**Circular Dichroism Measurements.** A solution with the desired concentration of peptide **1** was sonicated and allowed to equilibrate at 25 °C as described above. At various time points, spectral measurements were taken on a Jasco-815 CD spectropolarimeter, using a quartz cell with a 1.0 mm path length and 4 s averaging times. The CD signals resulting from buffer alone were subtracted from the spectrum of each peptide solution.

**Thioflavin T Fluorescence Assay.** A ThT stock solution (1.0 mM) was prepared by dissolving 1.6 mg of ThT in 5 mL of Millipore water, filtered through a 0.2  $\mu$ m filter, and then diluted 10 times with 20 mM MOPS buffer. Solutions of desired concentrations of peptide **1** were sonicated according to the procedure above

and added to the ThT solution (total volume of 100  $\mu$ L) prior to equilibration and measurements. The fluorescence spectra were recorded on a Varian Cary Eclipse fluorescence spectrometer, with a 96-microwell plate reader. The excitation wavelength was 440 nm (slit width 5.0 nm), and the emission wavelength was 490 nm (slit width 5 nm). To correct the signals, the background fluorescence of the ThT solution without peptide was subtracted from the fluorescence intensities obtained for the samples.

**Cryo-TEM Imaging.** Samples for direct imaging of the aqueous dispersions were prepared in the controlled environment box ( $T = 0^\circ\text{C}$ ) of a vitrification robot (Vitrobot, FEI), as follows: a 5  $\mu$ L drop of the solution was deposited on a glow-discharged TEM grid (300-mesh Cu lacey substrate; Ted Pella, Ltd.). The excess liquid was automatically blotted with a filter paper, and the specimen was rapidly plunged into liquid ethane and transferred to liquid nitrogen, where it was kept until use. The samples were examined below  $-175^\circ\text{C}$  using an FEI Tecnai 12 G<sup>2</sup> TWIN TEM that operated at 120 kV in low-dose mode and with a few micrometers under focus to increase the phase contrast. The images were recorded with a Gatan charge-coupled device camera (model 794) and analyzed by Digital Micrograph software, version 3.1.

**Atomic Force Microscopy.** Silicon substrates with native oxide layer were cleaned using a freshly prepared piranha solution (solution of 3:7 30% H<sub>2</sub>O<sub>2</sub> and concentrated H<sub>2</sub>SO<sub>4</sub>) for 30 min followed by three immersions in Millipore water for 10 min (Caution: Piranha is a very strong oxidant and reacts violently with many organic materials). The peptide solution (60  $\mu$ M **1** in buffer pH 7) was put on the surface (10  $\mu$ L for 10 s), followed by drying under nitrogen flow. Atomic force microscopy (Solver-Pro, NTMDT, Ru) topography and phase images were acquired using noncontact tips (NSG03 NT-MDT, Ru (5.1 N m<sup>-1</sup>, 150 kHz, and 1.74 N m<sup>-1</sup>, 90 kHz, respectively)).

**Kinetic Replication Experiments.** Experiments were initiated by preparing mixtures containing **N** (250  $\mu$ M), the desired amounts of template **1**, and TCEP (5 mM) as a reducing agent, in a MOPS buffer at pH = 7. The reaction solution was sonicated according to the procedure described above. The experiments were carried out in a 30-well Teflon plate, in which each well was used to run the reaction for a different time. Reactions were initiated after different times of equilibration by adding **E** (250  $\mu$ M) to the wells up to a total volume of 50  $\mu$ L. The entire volume of one of the wells was removed at each studied time point, immediately quenched with 50% acetic acid in water, and stored frozen until analyzed by RP-HPLC (see chromatogram for example in Figure S5). The concentration of each compound, reactants or product, was calculated by comparison with the HPLC peak of a foreign ABA-labeled peptide with a known concentration. The initial rates of product formation were calculated from points taken during the first 10 min of each reaction. The replication order (*p*) values were calculated as described before,<sup>27,35</sup> from the plot of log[initial rate] as a function of log[1] at the beginning of each reaction.

**Conflict of Interest:** The authors declare no competing financial interest.

**Acknowledgment.** This research was supported by the European Research Council (ERC 259204). We acknowledge the E.J. Safra Center and COST action CM0703, and thank Dr. Einat Roth for the assistance in TEM measurements and analysis, and Dr. Riky Cohen-Luria for fruitful discussions.

**Supporting Information Available:** Additional figures (Figures S1–S5) describing the self-assembly of **1** to form the fibril structures, its solubility in aqueous solutions, and further characterization of the replication reactions. This material is available free of charge via the Internet at <http://pubs.acs.org>.

## REFERENCES AND NOTES

- Bong, D. T.; Clark, T. D.; Granja, J. R.; Ghadiri, M. R. Self-Assembling Organic Nanotubes. *Angew. Chem., Int. Ed.* **2001**, *40*, 988–1011.
- Scanlon, S.; Aggeli, A. Self-Assembling Peptide Nanotubes. *Nano Today* **2008**, *3*, 22–30.
- Khakshoor, O.; Nowick, J. S. Artificial  $\beta$ -Sheets: Chemical Models of  $\beta$ -Sheets. *Curr. Opin. Chem. Biol.* **2008**, *12*, 722–729.
- Childers, W. S.; Ni, R.; Mehta, A. K.; Lynn, D. G. Peptide Membranes in Chemical Evolution. *Curr. Opin. Chem. Biol.* **2009**, *13*, 652–659.
- Hauser, C. A. E.; Zhang, S. Designer Self-Assembling Peptide Nanofiber Biological Materials. *Chem. Soc. Rev.* **2010**, *39*, 2780–2790.
- Cavalli, S.; Albericio, F.; Kros, A. Amphiphilic Peptides and Their Cross-Disciplinary Role as Building Blocks for Nanoscience. *Chem. Soc. Rev.* **2010**, *39*, 241–263.
- Sadownik, J. W.; Leckie, J.; Ulijn, R. V. Micelle to Fiber Biocatalytic Supramolecular Transformation of an Aromatic Peptide Amphiphile. *Chem. Commun.* **2011**, *47*, 728–730.
- Branco, M. C.; Sigano, D. M.; Schneider, J. P. Materials from Peptide Assembly: Towards the Treatment of Cancer and Transmittable Disease. *Curr. Opin. Chem. Biol.* **2011**, *15*, 427–434.
- Matson, J. B.; Stupp, S. I. Self-Assembling Peptide Scaffolds for Regenerative Medicine. *Chem. Commun.* **2012**, *48*, 26–33.
- Krieg, E.; Rybtchinski, B. Noncovalent Water-Based Materials: Robust yet Adaptive. *Chem.—Eur. J.* **2011**, *17*, 9016–9026.
- Kwak, M.; Herrmann, A. Nucleic Acid Amphiphiles: Synthesis and Self-Assembled Nanostructures. *Chem. Soc. Rev.* **2011**, *40*, 5745–5755.
- Wang, C.; Wang, Z.; Zhang, X. Amphiphilic Building Blocks for Self-Assembly: From Amphiphiles to Supra-Amphiphiles. *Acc. Chem. Res.* **2012**, *45*, 608–618.
- Li, J.; Carnall, J. M. A.; Stuart, M. C. A.; Otto, S. Hydrogel Formation upon Photoinduced Covalent Capture of Macrocycle Stacks from Dynamic Combinatorial Libraries. *Angew. Chem., Int. Ed.* **2011**, *50*, 8384–8386.
- Faramarzi, V.; Niess, F.; Moulin, E.; Maaloum, M.; Dayen, J.-F.; Beafrand, J.-B.; Zanettini, S.; Doudin, B.; Giuseppone, N. Light-Triggered Self-Construction of Supramolecular Organic Nanowires as Metallic Interconnects. *Nat. Chem.* **2012**, *4*, 485–490.
- Schulman, R.; Yurke, B.; Winfree, E. Robust Self-Replication of Combinatorial Information via Crystal Growth and Scission. *Proc. Natl. Acad. Sci. U. S. A.* **2012**, *109*, 6405–6410.
- Von Kiedrowski, G. A Self-Reproducing Hexadeoxyribonucleotide. *Angew. Chem., Int. Ed. Engl.* **1986**, *98*, 932–934.
- Paul, N.; Joyce, G. F. Minimal Self-Reproducing Systems. *Curr. Opin. Chem. Biol.* **2004**, *8*, 634–639.
- Dadon, Z.; Wagner, N.; Ashkenasy, G. The Road to Non-Enzymatic Molecular Networks. *Angew. Chem., Int. Ed.* **2008**, *47*, 6128–6136.
- Vidonne, A.; Philp, D. Making Molecules Make Themselves – the Chemistry of Artificial Replicators. *Eur. J. Org. Chem.* **2009**, *5*, 583–588.
- Taran, O.; von Kiedrowski, G. Replicators: Components for Systems Chemistry. *Chem. Synth. Biol.* **2011**, *289*–319.
- Ashkenasy, G.; Jagasia, R.; Yadav, M.; Ghadiri, M. R. Design of a Directed Molecular Network. *Proc. Natl. Acad. Sci. U. S. A.* **2004**, *101*, 11872–10877.
- Sadownik, J. W.; Philp, D. A Simple Synthetic Replicator Amplifies Itself from a Dynamic Reagent Pool. *Angew. Chem., Int. Ed.* **2008**, *47*, 9965–9970.
- Nguyen, R.; Allouche, L.; Buhler, E.; Giuseppone, N. Dynamic Combinatorial Evolution within Self-Reproducing Supramolecular Assemblies. *Angew. Chem., Int. Ed.* **2009**, *48*, 1093–1096.
- Samiappan, M.; Dadon, Z.; Ashkenasy, G. Replication NAND Gate with Light as Input and Output. *Chem. Commun.* **2011**, *47*, 710–712.
- Lee, D. H.; Granja, J. R.; Martinez, J. A.; Severin, K.; Ghadiri, M. R. A Self-Reproducing Peptide. *Nature* **1996**, *382*, 525–528.
- Issac, R.; Chmielewski, J. Approaching Exponential Growth with a Self-Reproducing Peptide. *J. Am. Chem. Soc.* **2002**, *124*, 6808–6809.
- Dadon, Z.; Samiappan, M.; Safranchik, E. Y.; Ashkenasy, G. Light-Induced Peptide Replication Controls Logic Operations in Small Networks. *Chem.—Eur. J.* **2010**, *16*, 12096–12099.
- Rubinov, B.; Wagner, N.; Rapaport, H.; Ashkenasy, G. Self-Reproducing Amphiphilic  $\beta$ -Sheet Peptides. *Angew. Chem., Int. Ed.* **2009**, *48*, 6683–6686.
- Rapaport, H.; Kjaer, K.; Jensen, T. R.; Leiserowitz, L.; Tirrell, D. A. Two-Dimensional Order in  $\beta$ -Sheet Peptide Monolayers. *J. Am. Chem. Soc.* **2000**, *122*, 12523–12529.
- Rapaport, H. Ordered Peptide Assemblies at Interfaces. *Supramol. Chem.* **2006**, *18*, 445–454.
- Mehta, A. K.; Lu, K.; Childers, W. S.; Liang, Y.; Dublin, S. N.; Dong, J.; Snyder, J. P.; Pingali, S. V.; Thiagarajan, P.; Lynn, D. G. Facial Symmetry in Protein Self-Assembly. *J. Am. Chem. Soc.* **2008**, *130*, 9829–9835.
- Pashuck, E. T.; Stupp, S. I. Direct Observation of Morphological Transformation from Twisted Ribbons into Helical Ribbons. *J. Am. Chem. Soc.* **2010**, *132*, 8819–8821.
- Aggeli, A.; Nyrkova, I. A.; Bell, M.; Harding, R.; Carrick, L.; McLeish, T. C. B.; Semenov, A. N.; Boden, N. Hierarchical Self-Assembly of Chiral Rod-Like Molecules as a Model for Peptide Beta-Sheet Tapes, Ribbons, Fibrils, and Fibers. *Proc. Natl. Acad. Sci. U. S. A.* **2001**, *98*, 11857–11862.
- Mihara, H.; Matsumura, S.; Takahashi, T. Construction and Control of Self-Assembly of Amyloid and Fibrous Peptides. *Bull. Chem. Soc. Jpn.* **2005**, *78*, 572–590.
- von Kiedrowski, G. Minimal Replicator Theory. I. Parabolic versus Exponential Growth. *Bioorg. Chem. Front.* **1993**, *3*, 113–146.
- Wagner, N.; Ashkenasy, G. Systems Chemistry: Logic Gates, Arithmetic Units and Network Motifs in Small Networks. *Chem.—Eur. J.* **2009**, *15*, 1765–1775.
- Sindi, S. S.; Serio, T. R. Prion Dynamics and the Quest for the Genetic Determinant in Protein-Only Inheritance. *Curr. Opin. Microbiol.* **2009**, *12*, 623–630.

38. Aguzzi, A.; Calella, A. M. Prions: Protein Aggregation and Infectious Diseases. *Physiol. Rev.* **2009**, *89*, 1105–1152.
39. Morris, A. M.; Watzky, M. A.; Finke, R. G. Protein Aggregation Kinetics, Mechanism, and Curve-Fitting: A Review of the Literature. *Biochim. Biophys. Acta, Proteins Proteomics* **2009**, *1794*, 375–397.
40. Cohen, F. E.; Pan, K. M.; Huang, Z.; Baldwin, M.; Fletterick, R. J.; Prusiner, S. B. Structural Clues to Prion Replication. *Science* **1994**, *264*, 530–531.
41. Brack, A. From Interstellar Amino Acids to Prebiotic Catalytic Peptides: A Review. *Chem. Biodiversity* **2007**, *4*, 665–679.
42. Maury, C. P. J. Self-Propagating  $\beta$ -Sheet Polypeptide Structures as Prebiotic Informational Molecular Entities: The Amyloid World. *Orig. Life Evol. Biosph.* **2009**, *39*, 141–150.
43. Williams, R. J.; Smith, A. M.; Collins, R.; Hodson, N.; Das, A. K.; Ulijn, R. V. Enzyme-Assisted Self-Assembly under Thermo-dynamic Control. *Nat. Nanotechnol.* **2009**, *4*, 19–24.
44. Carnall, J. M. A.; Waudby, C. A.; Belenguer, A. M.; Stuart, M. C. A.; Peyralans, J. J. P.; Otto, S. Mechanosensitive Self-Replication Driven by Self-Organization. *Science* **2010**, *327*, 1502–1506.
45. Weissbuch, I.; Illos, R. A.; Bolbach, G.; Lahav, M. Racemic Beta-Sheets as Templates of Relevance to the Origin of Homochirality of Peptides: Lessons from Crystal Chemistry. *Acc. Chem. Res.* **2009**, *42*, 1128–1140.